Adsorption 4, 187–195 (1998)

The Pore Structure Determination of Carbon Aerogels

Y. HANZAWA AND K. KANEKO
Physical Chemistry, Material Science, Graduate School of Science and Technology, Chiba University, 1-33 Yayoi-cho, Inage-ku, Chiba 263, Japan

N. YOSHIZAWA
Carbon Materials Laboratory, National Institute for Resources and Environment, 16-3 Onogawa, Tsukuba, Ibaraki 305, Japan

R.W. PEKALA
Lawrence Livermore National Laboratory, Livermore, CA 94550, USA

M.S. DRESSELHAUS
Department of Electrical Engineering and Computer Science and Department of Physics, Massachusetts Institute of Technology, Cambridge, MA 02139, USA

Abstract. The detailed adsorption isotherms of nitrogen on carbon aerogels at 77 K were measured. The N_2 adsorption isotherm had a marked hysteresis. The adsorption isotherms were analyzed by high resolution α_s-plots to evaluate their porosity. The α_s-plots showed an explicit upward deviation from the linearity below $\alpha_s = 0.5$, suggesting the presence of micropores. The mesoporosity and microporosity were separately determined from the α_s-plot. The predominant pores in carbon aerogels were mesopores and the percentage of micropores was in the range of 5 to 10% of the total pore volume. The N_2 adsorption hysteresis was analyzed with the Saam-Cole theory under the assumption of the cylindrical pore shape. The parameters determined from the Saam-Cole method were associated with the carbon aerogel structure.

Keywords: mesopore structure, Saam-Cole theory, adsorption hysteresis, carbon aerogel, nitrogen adsorption.

1. Introduction

Oxide aerogels are highly porous materials, consisting either of silica, alumina, titania or zirconia oxide, or mixtures of these oxides (Fricke, 1986). Mechanical properties of aerogels are directly associated with their higher order structure of primary particles and are a prerequisite to develop a new technology based on these materials. The pore structure plays an essential role in their properties. The preparation of aerogels starts with the controlled conversion of sol into gel, such as the growth of clusters or polymer chains from a chemical solution, the cross-linking of the primary entities, and the formation of a network. A supercritical drying allows the liquid to drain from the delicate gel structure without any collapse or shrinkage caused by surface tension of the liquid at evaporation. The resultant aerogels have a great possibility for new functioned materials.

Recently carbon aerogels were prepared from the pyrolysis of organic aerogels by Pekala and his coworkers; their thermal properties, electronic conductivity, photoconductivity and gas permeability were actively studied (Pekala and Kong, 1989; Pekala and Alviso, 1992; Pekala et al., 1992; Fung et al., 1994). Carbon aerogels have a three-dimensional network

structure made of interconnected uniform carbon particles. The predominant pores are mesopores. However, the presence of micropores has been suggested to have relevance to their physical properties. As the micropores should come from their particle connective parts and/or inherent micropores in the primary carbon particles, a quantitative determination of microporosity is quite important. Kaneko et al. have studied how to evaluate the microporosity of porous carbons of poor crystallinity using different approaches (Kaneko and Ishii, 1992; Kaneko et al., 1992; Setoyama et al., 1993; Ruike et al., 1994; Iiyama et al., 1995; Setoyama et al., 1996). The subtracting pore effect (SPE) method using high resolution α_s-plots for N_2 adsorption isotherms at 77 K can evaluate correctly the micropore structure (Kaneko et al., 1992; Gregg and Sing, 1982). Accordingly, the application of high resolution α_s-analysis should provide reliable information on the microporosity of carbon aerogels. The high resolution α_s-analysis was recently applied to study the pore structure of activated carbon aerogels, giving a quantitative determination of the microporosity and the mesoporosity of these materials (Hanzawa et al., 1996). The mesopore size distribution has also been determined by the N_2 adsorption isotherm using DH (Dollimore and Heal, 1964; Dollimore and Heal, 1970) or BJH method (Barrett et al., 1951). The traditional determination method for the mesopore size distribution is derived from capillary condensation theory which is based mainly on the adsorbate-adsorbate interaction, because the contact angle term is often neglected. Not only the interadsorbate interaction, but also the adsorptive-mesoporous surface interaction should be explicitly taken into account. The Saam-Cole theory (Saam and Cole, 1975; Bonnetain et al., 1988; Findenegg et al., 1993; Findenegg et al., 1994), which includes both interactions can provide important information on the nature of the surface and molecule. Furthermore, the Saam-Cole theory can be used to evaluate the mesoporosity.

In the present work, we determined the pore structures of carbon aerogels from the high resolution α_s-plot analysis, the Dubinin-Radushkevich analysis (Dubinin, 1960 and 1966) and the Saam-Cole analysis, in addition to the DH analysis.

2. Experimental

The carbon aerogels used in this study are prepared by Pekala's method (Pekala and Alviso, 1992; Pekala et al., 1992), derived from the sol-gel polymerization of resorcinol and formaldehyde with sodium carbonate as the base catalyst. The [resorcinol]/[catalyst] ratio was 200 and the aerogel density was controlled by varying the reactant concentration of the starting solution. The carbon aerogel was obtained by the supercritical drying of resorcinol-formaldehyde gel, subsequently followed by pyrolysis at 1323 K in a nitrogen atmosphere. The apparent density was determined from the weight and volume measurements of the bulk sample. The carbon aerogel sample is denoted by CA-*x* in this article, where *x* is associated with the apparent density.

The adsorption isotherm of nitrogen was measured gravimetrically at 77 K with the aid of a computer-aided apparatus. The samples were evacuated at 383 K and 1 MPa for 2 h prior to the adsorption measurements. The adsorption measurement was followed by desorption measurements under the same condition. It took about 30 h to measure both branches of the adsorption isotherm.

Transmission electron microscopy (TEM) measurements on carbon aerogels were performed using a Philips CM30 instrument operating at 100 kV. Specimens for TEM were prepared by crushing small pieces of carbon aerogels in the agate mortar and dispersing the materials with distilled water.

3. Results and Discussion

3.1. Higher Order and Pore Structures

Carbon aerogel samples were obtained in bulk form. Figure 1 shows pictures of the resorcinol-formaldehyde aerogel before pyrolysis at 1323 K and the resulting carbon aerogel after pyrolysis. Although this carbon aerogel has a monolith form and a glittering appearance, it has highly developed pores, as described later.

Transmission electron micrographs of CA-0.4 and CA-0.6 are shown in Fig. 2. For the CA-0.4 sample, carbon particles of diameter of 4–9 nm form an interconnecting network structure. The particles of 4–11 nm diameter for CA-0.6 are agglomerated with each other to form a more dense structure than CA-0.4.

The apparent density is shown in Table 1. The apparent density of the carbon aerogel used in this work is in the range of 0.30–0.58 $g \cdot cm^{-3}$. The true density of the carbon aerogels was 1.91 $g \cdot cm^{-3}$, as measured by the benzene replacement method. These densities indicated the highly porous structure of carbon aerogels.

Table 1. Pore structures of carbon aerogels.

Sample	Density ($g \cdot cm^{-3}$)	a_t ($m^2 \cdot g^{-1}$)	V_t ($ml \cdot g^{-1}$)	Micropore		Mesopore	
				a_{mi} ($m^2 \cdot g^{-1}$)	V_{mi} ($ml \cdot g^{-1}$)	a_{ms} ($m^2 \cdot g^{-1}$)	V_{ms} ($ml \cdot g^{-1}$)
CA-0.6	0.58	653	1.04	309	0.11	344	0.93
CA-0.4	0.43	577	1.51	222	0.08	355	1.43
CA-0.3	0.30	424	[0.82]*	100	0.04	324	[0.78]*

*[ ] was estimated from the obtained value at $P/P_0 = 0.992$.

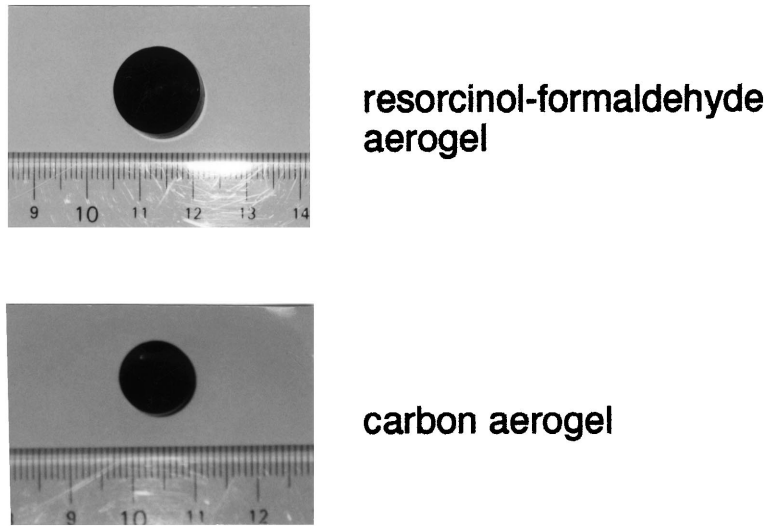

Figure 1. A resorcinol-formaldehyde aerogel and a carbon aerogel.

The adsorption isotherms of nitrogen on carbon aerogels are shown in Fig. 3. The adsorption isotherms of CA-0.6 and CA-0.4 are of type-IV and have a clear hysteresis. The hysteresis of CA-0.4 and CA-0.6 are of type-H1 and type-H2, respectively. The shape of the hysteresis loop is indicative of the type of pores present (Gregg and Sing, 1982; Sing et al., 1985). In the type-H1, the adsorption and desorption branches are almost vertical and nearly parallel over an appreciable range of gas uptake. This H1 type is often associated with the porous material, consisting of agglomerates or compacts of approximately uniform spheres in a fairly regular array and having a narrow distribution of pore size. The type-H2 loop is shown by many porous systems, but in this case the pore size and shape have a wider distribution than those of H1. The shape of the hysteresis loop is consistent with the aerogel model proposed from the TEM observations (Pekala and Kong, 1989; Pekala and Alviso, 1992). The TEM observation in this work also supports the previous model. The pore structure of CA-0.6 becomes less ordered, and the primary carbon spheres are packed closer together with a less regular network between the pores compared with CA- 0.4 (Hulsey et al., 1992). The adsorption isotherm of CA-0.3 is of type-IV having only a slight hysteresis. The density of CA-0.3 is the smallest, indicating a greater interparticle network than others; the pore size is distributed from mesopore to macropore ranges.

The α_s-plot analysis which was originally proposed by Sing (Gregg and Sing, 1982) is quite useful for micropore structure determination. Kaneko et al. analyzed the α_s-plot in the low α_s-region and developed the SPE-method (Kaneko et al., 1992). The SPE-method was applied to evaluate the micropore size distribution using the Grand Canonical Monte Carlo simulation (Setoyama et al., in press). The α_s-plots of the adsorption isotherms of nitrogen on carbon aerogels, based on a standard α_s-curve for nonporous carbon, are shown in Fig. 4 (Kaneko and Ishii, 1992; Gregg and Sing, 1982). The slopes of the straight line through

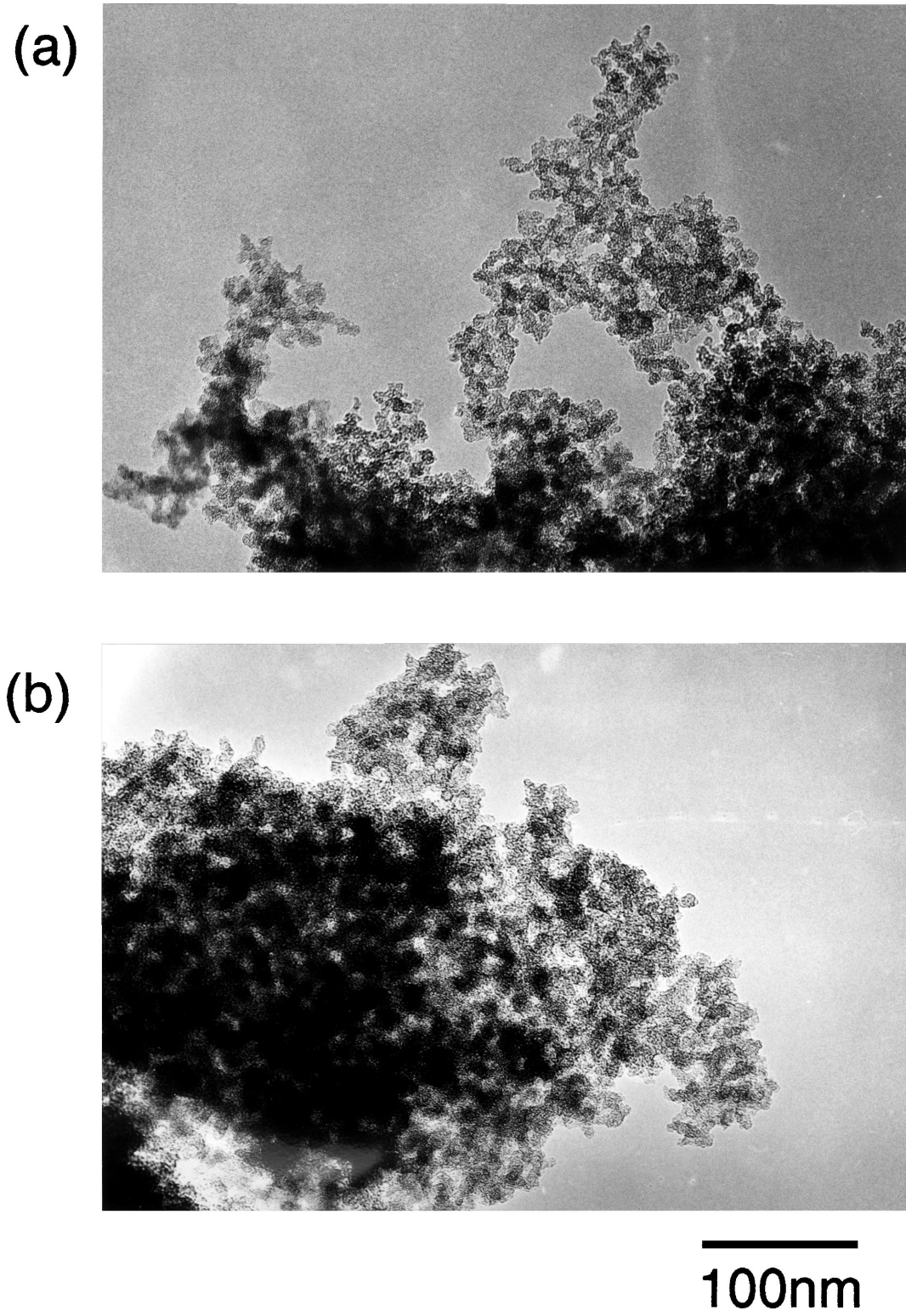

Figure 2. Transmission electron micrographs of (a) CA-0.4 and (b) CA-0.6.

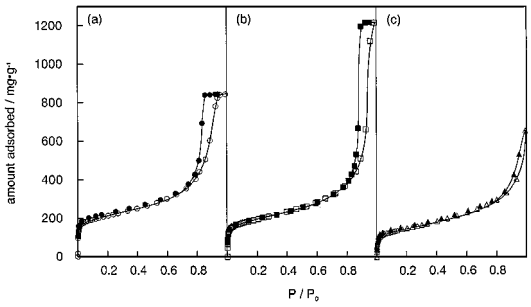

Figure 3. Adsorption isotherms of nitrogen on carbon aerogels at 77 K. Solid symbols denote desorption. (a) CA-0.6; (b) CA-0.4; (c) CA-0.3.

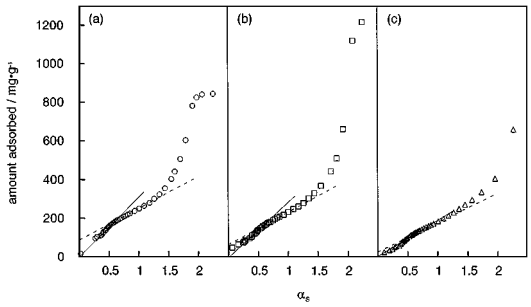

Figure 4. α_s-plots for the adsorption isotherms of nitrogen at 77 K. (a) CA-0.6; (b) CA-0.4; (c) CA-0.3. Points are experimental. The slopes of solid line and broken line gives the total surface area and mesoporous surface area.

the origin and the line in the high α_s region give the total surface area and mesoporous surface area, respectively. The extrapolation of the line in the high α_s region to the longitudinal axis leads to the micropore volume. In the very high relative pressure region, the adsorption isotherms of carbon aerogels are almost horizontal except for CA-0.3. This means that the pore filling is complete at the upper end of the hysteresis loop. The final amount of adsorption corresponds approximately to the total pore volume, and if the external surface area is negligible, the microporous surface area and mesopore volume are obtained by the subtraction of observable values of mesoporous surface area and micropore volume. These values of porosities are listed in Table 1. The contribution of micropores becomes greater as the apparent density increases. The micropore volume is 5–10% of the total pore volume, while the surface area of the micropores noticeably contributes to the total surface area (24–47%). These carbon aerogels have almost similar specific surface area for their mesopores. This is consistent with the dependence of the density on the number of particles per unit weight. The micropores in the primary particles themselves of the carbon aerogels, which originate from the structure of the precursor, shrink by pyrolysis, to cause a decrease in the micropore volume (Hulsey et al., 1992). The apparent density indicates that CA-0.3 has a greater pore volume than CA-0.4. As an accurate assessment of the pore volume of wider pores is quite difficult to make, the pore volume of CA-0.3 was estimated from the observed value at $P/P_0 = 0.992$.

Dubinin-Radushkevich (DR) analysis was used to determine the micropore volume in carbon aerogels. The DR equation is expressed as follows (Dubinin, 1960, 1966);

$$\ln W = \ln W_0 - (A/\beta E_0)^2 \tag{1}$$

where W_0 is the micropore volume, E_0 is a characteristic adsorption energy and A is Polanyi's adsorption potential defined as $A = RT \ln(P_0/P)$. β is an affinity coefficient related to the adsorbate-adsorbent interaction (β for $N_2 = 0.33$). The DR plots of carbon aerogels are shown in Fig. 5. The deviation from linearity near the longitudinal axis arises from the adsorption on the nonmicropore surfaces. The micropore volume W_0 and βE_0 are listed in Table 2. The micropore volume derived from DR analysis is larger than those from α_s-analysis. This is because the micropore volume from the DR plot includes the contribution of the adsorption in mesopores.

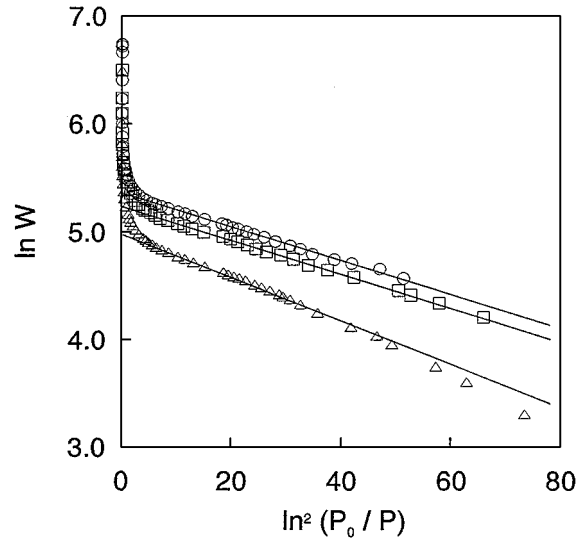

Figure 5. DR plots of nitrogen adsorption isotherms on carbon aerogels. (circle), CA-0.6; (square), CA-0.4; (triangle), CA-0.3.

Table 2. Parameters derived from DR analysis.

Sample	βE_0 (kJ · mol^{-1})	W_0 (ml · g^{-1})
CA-0.6	5.1	0.26
CA-0.4	5.1	0.23
CA-0.3	4.4	0.19

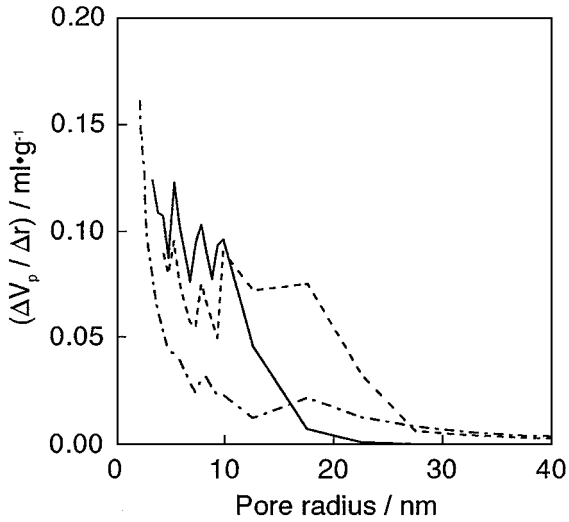

Figure 6. Pore size distribution of carbon aerogels based on the adsorption branch. Solid line, CA-0.6; broken line, CA-0.4; dash-dotted line, CA-0.3.

The pore size distribution of carbon aerogels derived from the adsorption branch of the isotherm was calculated using the Dollimore and Heal method (Dollimore and Heal, 1964, 1970), as shown in Fig. 6. The pore size distribution curve shifts to a large size as the apparent density decreases. The pore size of carbon aerogels is distributed in the wide region; 5–18 nm for CA-0.6 and 5–28 nm for CA-0.4. These values are larger than the average pore radius, which is calculated geometrically using the pore volume and surface area obtained from the α_s-analysis. The curve for CA-0.3 shows a pore size distribution over a wider range. The TEM observation in Fig. 2 indicates that the mesopore size is comparable to the primary particles size (4–11 nm in diameter). We must be cautious for evaluation of the pore size by simple observation of the TEM image. The two-dimensionally projected image tends to underestimate the average pore size. However, the discrepancy between the pore size from the Dollimore-Heal method and that from the TEM is still too serious. We need to search a new evaluation method of the pore size.

3.2. Pore Size Determination from the Saam-Cole Analysis and Pore Structure

The state of the fluid in mesopores is described in terms of macroscopic concepts such as surface tension, contact angle and the pressure difference across the curved meniscus, which leads to the Kelvin equation. The Kelvin equation has been helpful in analyzing the mesopore structure. The Kelvin approach can take into account the multilayer adsorption on the mesopore surface before capillary condensation. In case of a cylindrical mesopore of radius R and an adsorbed multilayer of the thickness l, the effective radius a can be used instead of the pore radius R. Here $a = R - l$. The modified Kelvin equation using a has been applied to the determination of the mesopore size distribution.

The Saam-Cole (SC) theory takes into account the effect of the multilayer adsorption more strictly (Saam and Cole, 1975; Bonnetain et al., 1988; Findenegg et al., 1993, 1994). The SC theory assumes the presence of the transition between the multilayer adsorbed phase and the condensed phase, that is, the liquid film. The stability of the liquid film in the pore is evaluated from (1) the long-range van der Waals interaction between the wall and film and (2) the curvature energy of the liquid/vapor interface. The curved film becomes unstable when the film thickness reaches a critical value l_c and pore condensation occurs at the vapor pressure corresponding to this film thickness. However, there is a metastable region of the multilayer film in the film width range of $l_m < l < l_c$. In this metastable region, the two-phase equilibrium of the pore fluid with a film of thickness l_m is actually more stable than a film of uniform thickness l_c. The SC theory gives a diagram of the regions of stability, metastability, and instability of the film in terms of the reduced variable $y = (R - l)/R = a/R$ as a function of the dimensionless pore radius R/R_0, where $R_0 = (3\pi\alpha\Delta\rho/\gamma)^{1/2}$ is a scaling parameter depending on the strength of the attractive adsorbate-wall interaction α (derived from a Frenkel-Halsey-Hill (FHH) plot: $\ln(P_0/P) = a/l^3$), the difference in densities $\Delta\rho$ of liquid and coexistent vapor, and the surface tension γ of the liquid forming the film. For large a (i.e., wide pores and/or relatively thin films), the border lines separating the regions of stability, metastability, and instability are approximately given by following equations:

$$\left(\frac{R}{R_0}\right)_c = \frac{y_c}{\sqrt{\pi}(1-y_c)^2} = \frac{1-\frac{l_c}{R}}{\sqrt{\pi}\left(\frac{l_c}{R}\right)^2} \qquad (2)$$

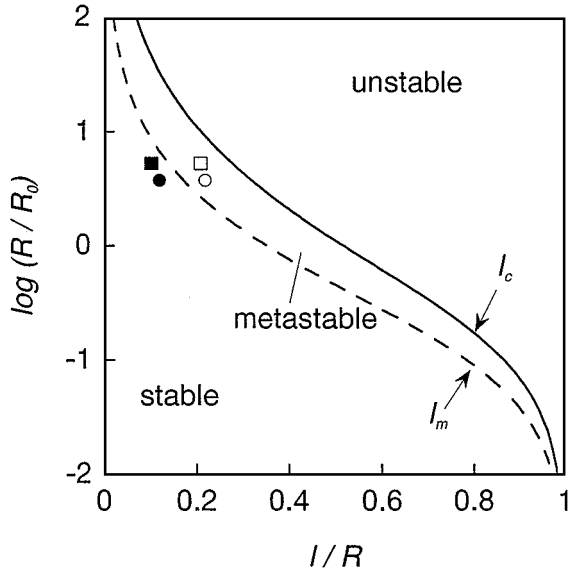

Figure 7. The Saam-Cole phase diagram of the thin adsorbed film in a cylindrical pore. Open symbols denote l_c and solid symbols denote l_m. (circle), CA-0.6; (square), CA-0.4.

$$\left(\frac{R}{R_0}\right)_m = \frac{y_m}{\sqrt{3\pi}(1-y_m)^{3/2}} = \frac{1-\frac{l_m}{R}}{\sqrt{3\pi}\left(\frac{l_m}{R}\right)^{3/2}} \quad (3)$$

For an isotherm of a certain system (constant R and R_0), a horizontal line of $y = R/R_0$ in the phase diagram of Fig. 7 passes through the curves at two points, giving the values of the thickness at which the condensation and evaporation begin. In the adsorption process, the adsorption isotherm starts in the region of stable films at a small l/R, extending into the region of the thick metastable film up to the borderline of instability, where a vertical ascending step appears in the adsorption isotherm due to pore filling. In the desorption, a vertical descending step occurs at the border between the metastable and stable regions.

The phase diagram of the SC theory gives information on the pore structure. On testing whether the pore condensation results on carbon aerogels conform to the phase diagram of the SC theory, the value l_m (metastability limit) can be taken as the film thickness at the lower closure point of the hysteresis loop. The value l_c (instability limit) is derived from the adsorption branch of the hysteresis loop as the point at which the ascending curve reaches a limiting constant slope. The van der Waals interaction parameter is derived from the FHH analysis of the film thickness l as a function of the relative pressure P/P_0. The average pore radius

Table 3. Experimental limits of stability.

Sample	R_{ave} (nm)*	α_{FHH} (10^{-25} $Jm^3 \cdot mol^{-1}$)	R_0 (nm)†	l_c (nm)	l_m (nm)
CA-0.6	5.42	0.716	1.44	1.18	0.65
CA-0.4	8.04	0.795	1.52	1.68	0.83

*With cylindrical pore, $R_{ave} = 2V_{ms}/a_{ms}$.
†For nitrogen at 77 K, $\Delta(1/V_m) = 27.3$ mmol $\cdot$ cm^{-1} and $\gamma = 8.85$ mN $\cdot$ m^{-1}.

R_{ave} was derived from the geometrical calculation of the pore volume and the surface area using the cylindrical model. These values are listed in Table 3. The Saam-Cole plots with the resulting values of l_m/R and l_c/R for CA-0.6 and CA-0.4 are shown in Fig. 7, with the predicted limits of metastability and instability by the Saam-Cole theory. Although the cylindrical model seems to be unsuitable for representing the pore structure of carbon aerogels, both l_m/R and l_c/R values well agree with predicted curves. The values of l_c and l_m corresponding to R/R_0 on the predicted curves are 1.73 and 0.94 nm for CA-0.6, and 2.23 and 1.13 nm for CA-0.4, respectively. The disagreements should be caused by an incorrect value for the average pore radius as R_{ave}.

We can calculate the best pore radius R_{calc} satisfying Eq. (2) or (3) using the observed R_0, l_c, and l_m values. As it is difficult to get a solution for R_{calc} analytically from Eq. (2) or (3), we searched for an approximate solution for R^c_{calc} and R^m_{calc} from Eqs. (4) and (5), respectively.

$$\left|\frac{R}{R_0} - \frac{1-\frac{l_c}{R}}{\sqrt{\pi}\left(\frac{l_c}{R}\right)^2}\right| \to 0 \quad (4)$$

$$\left|\frac{R}{R_0} - \frac{1-\frac{l_m}{R}}{\sqrt{3\pi}\left(\frac{l_c}{R}\right)^{3/2}}\right| \to 0 \quad (5)$$

However, to get an approximate solution from Eqs. (4) and (5) is not easy. Then we use Eqs. (6) and (7) to provide reliable approximate solutions for Eqs. (2) and (3).

$$\log\left|\frac{R}{R_0} - \frac{1-\frac{l_c}{R}}{\sqrt{\pi}\left(\frac{l_c}{R}\right)^2}\right| \to -\infty \quad (6)$$

$$\log\left|\frac{R}{R_0} - \frac{1-\frac{l_m}{R}}{\sqrt{3\pi}\left(\frac{l_c}{R}\right)^{3/2}}\right| \to -\infty \quad (7)$$

Table 4. Comparison of pore radii obtained by different methods.

Sample	R_{ave} (nm)	R^c_{calc} (nm)	R^c_{Kelvin} (nm)	R^m_{calc} (nm)	R^m_{Kelvin} (nm)
CA-0.6	5.42	2.89	8.88	2.37	3.08
CA-0.4	8.04	4.97	15.9	3.81	5.27

The obtained R_{calc} values are collected in Table 4 together with the pore radii calculated by the following modified Kelvin equation (Dollimore and Heal, 1970) for l_c and l_m:

$$R_{Kelvin} = r_K + t \tag{8}$$
$$t = 0.354\left(\frac{-5}{\ln P/P_0}\right)^{1/3}$$

where r_K is the Kelvin radius at complete wetting and t is the thickness of an adsorbed film at relative pressure P/P_0 in nanometers. The values of R_{ave}, R^c_{calc}, and R^c_{Kelvin} that are determined by different ways are different from each other (see Table 4). As the mesopore shape of carbon aerogel cannot be geometrically described, it is reasonable that the three values do not coincide with each other. However, both R^c_{calc} and R^m_{calc}, which were calculated by use of the observed quantities of l_c, l_m and R_0, are close to each other. This fact indicates the goodness of the Saam-Cole analysis. Then the thermodynamic approach to capillary condensation is indispensable for describing the pore structure correctly. Moreover, we examined the agreement between the observed l_c and calculated one, $l_{c,calc}$, using both R_0 and R^m_{calc} with the aid of Eq. (2). In the same way, l_m was compared with $l_{m,calc}$ calculated from R_0 and R^c_{calc} with Eq. (3). These values were listed in Table 5. The secondary obtained values $l_{c,calc}$ and $l_{m,calc}$ are consistent with the experimental values of l_c and l_m, suggesting the goodness of the Saam-Cole approach. The average pore size geometrically calculated using the adsorption data for the pore volume and surface area is useful and has been widely used for the characterization of many porous materials. However, the geometrically calculated average pore size does not express the true pore structure in a three-dimensional network system such as these carbon aerogels. This Saam-Cole analysis can give the correct pore size.

Table 5. Comparison of film thickness.

Sample	l_c (nm)	$l_{c,calc}$ (nm)	l_m (nm)	$l_{m,calc}$ (nm)
CA-0.6	1.18	1.04	0.65	0.71
CA-0.4	1.68	1.43	0.83	0.93

Conclusions

The N_2 adsorption isotherm of carbon aerogels having a marked hysteresis was analyzed by high resolution α_s-plots to evaluate their porosity. A remarkable upward deviation from linearity below $\alpha_s = 0.5$ in the α_s- plots showed the presence of micropores. The microporosity was quantitatively determined from the α_s-plot. The predominant pores in carbon aerogels are mesopores and the percentages of micropores are in the range of 5–10% of the total pore volume. The conventional pore size distribution analysis from the adsorption branch does not give a satisfactory picture of the pore structure. The self consistent analysis using Saam-Cole theory leads to a reasonable average pore size determination for the three-dimensionally intersecting pore system.

Nomenclature

A	Polanyi's adsorption potential defined ($= RT \ln(P_0/P)$)
a	Effective radius of pore ($= R - l$)
a_{mi}	Microporous surface area
a_{ms}	Mesoporous surface area
a_t	Total surface area
E_0	Characteristic adsorption energy
l	Thickness of adsorbed film
l_c	Film thickness of stability limit
$l_{c,calc}$	Calculated film thickness of stability limit
l_m	Film thickness of instability limit
$l_{m,calc}$	Calculated film thickness of instability limit
P/P_0	Relative pressure
R	Pore radius
R_{ave}	Average pore size derived from gerometrical calculation ($= 2v_{ms}/a_{ms}$)
R^c_{calc}	Calculated pore radius using R_0 and l_c
R^c_{Kelvin}	Calculated pore radius for l_c using modified Kelvin equation
R^m_{calc}	Calculated pore radius using R_0 and l_m
R^m_{Kelvin}	Calculated pore radius for l_m using modified Kelvin equation
R_0	Scaling parameter ($= \sqrt{\frac{3\pi\alpha\Delta\rho}{\gamma}}$)

t	Film thickness of an adsorbed layer
V_{mi}	Micropore volume
V_{ms}	Mesopore volume
V_t	Total pore volume
W_0	Micropore volume in DR analysis
y	Reduced variable ($= \frac{(R-l)}{R} = \frac{a}{R}$)

Greek Letters

α	Attractive adsorbate-wall interaction derived from FHH analysis
α_s	α_s value
β	Affinity coefficient (0.33 for N_2)
$\Delta\rho$	Difference in densities of liquid and coexistent vapor
γ	Surface tension

Acknowledgment

This work was supported by a Grant-in-Aid for Scientific Research on Priority Area (Carbon Alloy: No. 08355027) by the Ministry of Education, Science and Culture, Japanese Government.

References

Barrett, E.P., L.G. Joyner, and P.P. Halenda, "The Determination of Pore Volume and Area Distributions in Porous Substances. I. Computations from Nitrogen Isotherms," *J. Am. Chem. Soc.*, **73**, 373–380 (1951).

Bonnetain, L., J.L. Ginoux, and M. Cabedo, "Determination of Mesopores Diameters in Porous Solids from Adsorption Measurements—Criticisms and Suggestions," *Characterization of Porous Solids*, K.K. Unger, J. Rouquerol, K.S.W. Sing, and H. Kral (Eds.), pp. 223–232, Elsevier, Amsterdam, 1988.

Dollimore, D. and G.R. Heal, "An Improved Method for the Calculation of Pore Size Distribution from Adsorption Data," *J. Appl. Chem.*, **14**, 109–114 (1964).

Dollimore, D. and G.R. Heal, "Pore-Size Distribution in Typical Adsorbent Systems," *J. Colloid Interface Sci.*, **33**, 508–519 (1970).

Dubinin, M.M. "The Potential Theory of Adsorption of Gases and Vapores for Adsorbents with Energetically Nonunifrom Surfaces," *Chem. Rev.*, **60**, 235–241 (1960).

Dubinin, M.M., "Porous Structures and Adsorption Properties of Active Carbons," *Chemistry and Physics of Carbon*, P.L. Walker (Ed.), Vol. 2, pp. 51–120, Marcel Dekker, New York, 1966.

Findenegg, G.H., S. Groß, and T. Michalski, "Multilayer Adsorption and Pore Condensation in Controlled-Pore Glass: A Test of the Saam-Cole Theory of Mesopore Filling," *Fundamentals of Adsorption*, M. Suzuki (Ed.), pp. 1961–1968, Kodansha, Tokyo, 1993.

Findenegg, G.H., S. Groß, and T. Michalski, "Pore Condensation in Controlled-Pore Glass: An Experimental Test of the Saam-Cole Theory," *Characterization of Porous Solids III*, J. Rouquerol, F. Rodoriguez-Reinoso, K.S.W. Sing, and K.K. Unger (Eds.), pp. 71–80, Elsevier, Amsterdam, 1994.

Fricke, J. (Ed.), *Aerogels*, Springer-Verlag, Berlin, 1986.

Fung, A.W.P., Z.H. Wang, M.S. Dresselhaus, G. Dresselhaus, R.W. Pekala, and M. Endo, "Coulomb-Gap Magnetotransport in Granular and Porous Carbon Structures," *Phys. Rev. B*, **49**, 17325–17335 (1994).

Gregg, S.J. and K.S.W. Sing, *Adsorption, Surface Area and Porosity*, 2nd edition, Academic Press, London, 1982.

Hanzawa Y., K. Kaneko, R.W. Pekala, and M.S. Dresselhaus, "Activated Carbon Aerogels," *Langmuir*, **12**, 6167–6169 (1996).

Hulsey, S.S., C.T. Alviso, F.M. Kong, and R.W. Pekala, "The Effect of Pyrolysis Temperature and Formation on Pore Size Distribution and Surface Area of Carbon Aerogels," *Mat. Res. Soc. Symp. Proc.*, **270**, 53–57 (1992).

Iiyama, T., K. Nishikawa, T. Otowa, and K. Kaneko, "An Ordered Water Molecular Assembly Structure in a Slit-Shaped Carbon Nanospace," *J. Phys. Chem.*, **99**, 10075–10076 (1995).

Kaneko, K. and C. Ishii, "Superhigh Surface Area Determination of Microporous Solids," *Colloid Surf.*, **67**, 203–212 (1992).

Kaneko, K., K. Shimizu, and T. Suzuki, "Intrapore Field Dependent Micropore Filling of Supercritical N_2 in Slit-shaped Micropores," *J. Chem. Phys.*, **98**, 8705–8711 (1992).

Pekala, R.W. and C.T. Alviso, "Carbon Aerogels and Xerogels," *Mat. Res. Soc. Symp. Proc.*, **270**, 3–14 (1992).

Pekala, R.W., C.T. Alviso, F.M. Kong, and S.S. Hulsey, "Aerogels Derived from Multifunctional Organic Monomers," *J. Non-Cryst. Solids*, **145**, 90–98 (1992).

Pekala, R.W. and F.M. Kong, "Resorcinol-Formaldehyde Aerogels and their Carbonized Derivatives," *Polym. Prpts.*, **30**, 221–223 (1989).

Ruike, M., T. Kasu, N. Setoyama, T. Suzuki, and K. Kaneko, "Inaccessible Pore Characterization of Less-Crystalline Microporous Solids," *J. Phys. Chem.*, **98**, 9594–9600 (1994).

Saam, F.W. and M.W. Cole, "Excitations and Thermodynamics for Liquid-Helium Films," *Phys. Rev. B*, **11**, 1086–1105 (1975).

Setoyama, N., K. Kaneko, and F. Rodoriguez-Reinoso, "Ultramicropore Characterization of Microporous Carbons by Low-Temperature Helium Adsorption," *J. Phys. Chem.*, **100**, 10331–10336 (1996).

Setoyama, N., M. Ruike, T. Kasu, T. Suzuki, and K. Kaneko, "Surface Characterization of Microporous Solids with He Adsorption and Small Angle X-ray Scattering," *Langmuir*, **9**, 2612–2617 (1993).

Setoyama, N., S. Suzuki, and K. Kaneko, "Simulation Study on Relationship between High Resolution α_s-Plot and Pore Size Distribution for Activated Carbons," *Carbon*, in press.

Sing, K.S.W., D.H. Everett, R.A.W. Haul, L. Moscou, R.A. Pierotti, J. Rouquerol, and T. Siemieniewska, "Reporting Physisorption Data for Gas/Solid Systems with Special Reference to the Determination of Surface Area and Porosity," *Pure Appl. Chem.*, **57**, 603–619 (1985).